



## Special Feature: Electronic and Optical Devices

Research Report

### Optical Amplification and Laser Oscillation Characteristics of Tb<sup>3+</sup>-doped Fluoride Glass Fiber

Tatsuya Yamashita and Yasutake Ohishi

Report received on May 16, 2011

**■ABSTRACT■** The spectroscopic properties of Tb<sup>3+</sup>-doped fluoride glass were comprehensively investigated to determine their feasibility as gain media in the 0.54 μm band. The radiative and non-radiative rates associated with the <sup>5</sup>D<sub>4</sub> → <sup>7</sup>F<sub>5</sub> transition of Tb<sup>3+</sup> were analyzed by Judd-Ofelt analysis. The amplification performance of a Tb<sup>3+</sup>-doped fluoride fiber operating in the 0.54 μm band was experimentally demonstrated, and the gain characteristics of the <sup>5</sup>D<sub>4</sub> → <sup>7</sup>F<sub>5</sub> transition were analyzed based on a numerical model. The experiments showed that the excited state absorption of the pump light dominates the gain characteristics for a Tb<sup>3+</sup>-doped fluoride fiber, and that improved gains of 8.3 dB and 15.5 dB could be successfully attained for single and double-cascaded Tb<sup>3+</sup>-doped fluoride fiber amplifiers, respectively, operating with bi-directional pumping. In addition, we demonstrated continuous-wave (CW) laser operation of a Tb<sup>3+</sup>-doped fluoride fiber laser at 542.8 nm, which we believe is the first example of CW laser operation with Tb<sup>3+</sup>-doped materials in the 0.54 μm band.

**■KEYWORDS■** Rare earth doped material, Optical amplifier, Fiber laser, Judd-Ofelt analysis, Fluoride glass

#### 1. Introduction

Several of the  $4f-4f$  transitions of rare earth ions can be utilized in obtaining efficient laser emissions and optical signal amplifications when these ions are doped into optical fibers and waveguides.<sup>(1)</sup> Many of the current efforts to develop rare earth-doped fibers have focused on applications for telecommunication systems operating in the infrared wavelength range. Recently, visible lasers have attracted much attention in several applications, including optical data storage, biochemical spectroscopy, and laser material processing. In addition, it is expected that optical amplification devices active in the green (0.54 μm) band will be required for plastic optical fiber communication networks for automobiles. This is because green LEDs based on GaN semiconductor technology possess advantages in terms of both high speed modulation characteristics and low-loss transmission in plastic optical fibers over conventional red LEDs based on InGaAs.<sup>(2)</sup>

One approach to obtaining visible laser and amplifiers is to use frequency upconversion processes in rare earth-doped fibers.<sup>(3)</sup> Among the rare earth ions that exhibit frequency upconversion emissions in the

visible wavelength range, Er<sup>3+</sup> is considered as one of the most efficient. The green emission originating from the <sup>4</sup>S<sub>3/2</sub> → <sup>4</sup>I<sub>15/2</sub> transition of Er<sup>3+</sup> has been observed in several glass systems with low phonon energies such as chalcogenide, fluoride, and tellurite glasses. However, a high pump power is required to create a population inversion state between the <sup>4</sup>S<sub>3/2</sub> and <sup>4</sup>I<sub>15/2</sub> levels of Er<sup>3+</sup>, since excitation of the <sup>4</sup>S<sub>3/2</sub> level is achieved by a sequential two-photon absorption process, that is, ground state absorption (GSA) and excited state absorption (ESA).

Tb<sup>3+</sup>-doped glasses are considered suitable candidates for gain media in the green (0.54 μm) band. In the case of Tb<sup>3+</sup>, the <sup>5</sup>D<sub>4</sub> → <sup>7</sup>F<sub>5</sub> transition acts as a four-level laser system allowing lower threshold for the pumping power in principle. In the 1960s, operation of a pulsed green laser was demonstrated with a Tb<sup>3+</sup> chelate in liquid solution using Xe flash pumping at room temperature.<sup>(4)</sup> However, to the best of our knowledge, demonstration of the continuous-wave (CW) laser action of Tb<sup>3+</sup> has not been demonstrated. One of the main problems associated with Tb<sup>3+</sup>-doped gain media is that the absorption cross sections of the <sup>7</sup>F<sub>6</sub> → <sup>5</sup>D<sub>4</sub> transitions for pumping are relatively small. In addition, a photodarkening effect,

which potentially degrades the gain performance, has been observed in Tb<sup>3+</sup>-doped germanosilicate and aluminosilicate glass fibers.<sup>(5)</sup> No attempts have been made to quantitatively investigate the signal amplification characteristics of Tb<sup>3+</sup>-doped materials.

In view of this background, the present study focuses on evaluating the potential application of Tb<sup>3+</sup>-doped materials as optical gain media in the 0.54 μm band. Surprisingly, there are no reports on the amplification characteristics of Tb<sup>3+</sup>, despite the fact that Tb<sup>3+</sup>-doped glass seems to be a possible gain medium for the green band.

It is thought that the photodarkening effect is caused by absorption from the <sup>5</sup>D<sub>4</sub> level to the 5*d* levels of Tb<sup>3+</sup>. Therefore, to avoid photodarkening as well as excited-state absorptions from the <sup>5</sup>D<sub>4</sub> level, it is very important to use a fiber material in which 5*d* absorption becomes as weak as possible. According to Dorenbos,<sup>(6)</sup> the 5*d* levels of Tb<sup>3+</sup> are at higher energies in fluoride materials than in oxide materials. Therefore, we selected ZrF<sub>4</sub>-based fluoride glass as a fiber material in this study.

In Section 2, Tb<sup>3+</sup>-doped fluoride glasses were synthesized, and their spectroscopic properties investigated to assess their potential application as gain media in the 0.54 μm band. In Section 3, signal amplification experiments were carried out using the Tb<sup>3+</sup>-doped fluoride fiber (TBDF) under 488 nm pumping. The amplification performance was analyzed based on an amplification model of the TBDF using the spectroscopic parameters obtained in Section 2. We discuss the importance of addressing the effects of signal ESA, pump ESA, and cooperative upconversion, which may seriously degrade the signal gain of the <sup>5</sup>D<sub>4</sub> → <sup>7</sup>F<sub>5</sub> transition. In addition, we demonstrate continuous-wave (CW) laser operation of a Tb<sup>3+</sup>-doped fluoride fiber laser at 542.8 nm. We believe that this is the first demonstration of CW laser operation with a Tb<sup>3+</sup>-doped material in the 0.54 μm band. The obtained results show that it is possible to construct optical amplifiers and fiber lasers in the 0.54 μm band using the Tb<sup>3+</sup>-doped fibers.

## 2. Spectroscopic properties of Tb<sup>3+</sup>-doped fluoride glasses

In this section, the spectroscopic properties of Tb<sup>3+</sup>-doped fluoride glasses are investigated to assess their potential as gain media in the 0.54 μm band. The spectroscopic parameters of Tb<sup>3+</sup>, such as the

spontaneous emission rates and the nonradiative relaxation rates of the excited states, as well as the emission cross sections, are very important for understanding their performance as gain media. Later we discuss the potential of Tb<sup>3+</sup>-doped fluoride glasses as gain media in the 0.54 μm band.

## 2.1 Experimental

### 2.1.1 Preparation of samples

The glass composition of fluoride glass used in this study is 51ZrF<sub>4</sub>-20BaF<sub>2</sub>-4.5LaF<sub>2</sub>-4.5AlF<sub>3</sub>-20NaF (ZBLAN) in mol%. Samples with Tb<sup>3+</sup> concentrations varying from 0.1 wt% to 5 wt% were prepared. The glass samples were obtained by a conventional melt-quenching method. The starting materials were 99.9% pure ZrF<sub>4</sub>, BaF<sub>2</sub>, LaF<sub>2</sub>, AlF<sub>3</sub>, NaF, and TbF<sub>3</sub>. Batches of the starting materials were melted in a platinum crucible set in an electronic furnace at 850°C for 1 hour. The furnace was purged with dry O<sub>2</sub> and N<sub>2</sub> at a flow rate of 3 l/min to prevent hydroxyl impurities. The melts were poured onto a steel plate preheated to around the glass transition temperature, and then annealed at the same temperature for 10 h in an electric furnace.

The obtained glasses were cut into specimens of approximately 15 mm × 15 mm × 5 mm and polished carefully to satisfy the requirements for optical measurement. Measurement of the density of the glasses was performed by the Archimedes method with water as the immersion fluid. The accuracy of the density was within ± 0.3%.

### 2.1.2 Optical measurements

The refractive indices of the samples were measured with a prism coupler system (Metricon, Model 2010) at wavelengths of 632.8, 974, 1320, and 1544 nm. The measured refractive indices were fitted to Sellmeier's dispersion formula in the following form:

$$n(\lambda)^2 = A + \frac{B\lambda^2}{\lambda^2 - C^2} - D\lambda^2, \dots \dots \dots (1)$$

where λ is the wavelength and the coefficients *A*, *B*, *C*, and *D* are constants. The above formula was used in the Judd-Ofelt analysis in order to theoretically calculate the oscillator strength. The values of the

parameters  $A$ ,  $B$ ,  $C$ , and  $D$  obtained for the ZBLAN glass doped with 2 wt%  $Tb^{3+}$  were 1.96989, 0.26669, 0.18047, and 0.00418, respectively, using micrometers ( $\mu m$ ) as the unit of wavelength.

The absorption spectra of the samples were measured with a UV-VIS-NIR double-beam spectrophotometer (Perkin-Elmer Lambda 900) in the spectral range of 300–3300 nm. The absorption cross section  $\sigma_a$  was determined from the measured absorbance  $\log_{10}(I/I_0)$  using the following relationship:

$$\sigma_a = \frac{\mu}{N_{Tb}} = \frac{2.303 \log_{10}(I/I_0)}{l N_{Tb}}, \dots \dots \dots (2)$$

where  $\mu$  is the absorption coefficient,  $l$  is the sample thickness, and  $N_{Tb}$  is the number of  $Tb^{3+}$  ions per unit volume.

In the emission decay measurements, an  $Ar^+$  ion laser at 488 nm was used as the excitation source for the  $^5D_4$  level of  $Tb^{3+}$ . Emission from the samples was measured with a monochromator equipped with a photomultiplier tube as a detector. The emission signal was detected using a lock-in amplifier. A digital oscilloscope was used to record the output signal from the detector. Emission lifetimes were obtained from the first  $e$ -folding time of the emission decay curve.

**2. 1. 3 Judd-Ofelt analysis**

It is important to know the transition probabilities, or oscillator strength, for the various transitions between energy levels in rare earth ions. Unfortunately, these are extremely difficult to measure, and must be calculated using Judd-Ofelt (J-O) theory.<sup>(7-9)</sup>

According to J-O theory, the free-ion states of rare earth metals are composed of linear combinations of Russell-Saunders (R-S) states which diagonalize the combined electrostatic and spin-orbit energy matrices. The effects of the Stark field of the host reduce the  $(2J + 1)$ -fold degeneracy of the free ion states and cause a small mixing of states. Because the effect of the Stark field on the  $4f^N$  configuration is small, it is treated as a perturbation of the free ion states. The calculated states have a configuration interaction included in the matrix to be diagonalized and this has the following form:

$$|f^N[\alpha SL]J\rangle = \sum_{\alpha', S', L'} C_{\alpha' S' L'} |f^N \alpha' S' L'\rangle, \dots \dots \dots (3)$$

where  $C_{\alpha' S' L'}$  are the coupling coefficients transforming the R-S states to intermediate coupling states.  $J$  is the quantized total angular momentum, and  $S$  and  $L$  are the quantized spin and orbital angular momenta, respectively. The symbol  $\alpha$  represents the additional quantum numbers that are needed to specify the  $4f^N$  states uniquely. Eigenfunctions for the  $4f$  states of  $Tb^{3+}$  were obtained by Caird, et al.<sup>(10)</sup>

Magnetic dipole transitions are partially allowed between  $4f^N$  states and subject to selection rules  $\Delta\alpha = S = 0$  and  $\Delta J = 0, \pm 1$  of the R-S limit. Under these conditions, the line strength for a magnetic dipole (md) transition between  $J$  states is given by

$$S_{md}(aJ; bJ') = \frac{\beta^2}{4} \left| \langle f^N[\alpha SL]J || \mathbf{L} + 2\mathbf{S} || f^N[\alpha' S' L']J' \rangle \right|^2, \dots \dots \dots (4)$$

where  $a$  and  $b$  denote  $S$ ,  $L$  and the other quantum numbers necessary to specify the eigenstate,  $\beta$  is equal to  $eh/2mc$ ,  $e$  is the elementary charge,  $h$  is Planck's constant,  $m$  is the electron mass,  $c$  is the velocity of light,  $L$  is the orbital angular momentum and  $S$  is the spin orbital angular momentum. The matrix elements of  $\langle\langle L + 2S \rangle\rangle$  are given by

$$\begin{aligned} J' = J & \\ \langle f^N[\alpha SL]J || \mathbf{L} + 2\mathbf{S} || f^N[\alpha' S' L']J \rangle & \\ = \delta(\alpha, \alpha') \delta(\beta, \beta') \delta(L, L') \beta \left\{ \frac{2J+1}{4J(J+1)} \right\}^{\frac{1}{2}} & \\ \{S(S+1) - L(L+1) + 3J(J+1)\}, & \\ J' = J - 1 & \\ \langle f^N[\alpha SL]J || \mathbf{L} + 2\mathbf{S} || f^N[\alpha' S' L']J - 1 \rangle & \\ = \delta(\alpha, \alpha') \delta(\beta, \beta') \delta(L, L') \beta & \\ \left[ \frac{\{S(S+L+1)^2 - J^2\} \{J^2 - (L-S)^2\}}{4J} \right]^{\frac{1}{2}}, & \\ J' = J + 1 & \\ \langle f^N[\alpha SL]J || \mathbf{L} + 2\mathbf{S} || f^N[\alpha' S' L']J + 1 \rangle & \\ = \delta(\alpha, \alpha') \delta(\beta, \beta') \delta(L, L') \beta & \\ \left[ \frac{\{S(S+L+1)^2 - (J+1)^2\} \{(J+1)^2 - (L-S)^2\}}{4(J+1)} \right]^{\frac{1}{2}} & \\ \dots \dots \dots & (5) \end{aligned}$$

The line strengths for the electric dipole (ed) transitions are calculated in J-O theory as the sum of the intensity parameters  $\Omega_t$  and the doubly reduced matrix elements of the tensor operator  $U(t)$  of rank  $t$ , with  $t = 2, 4, 6$  due to the selection  $|AJ| \cdot 2l$  and  $l = 3$  for rare earth elements, and are given by

$$S_{ed}(aJ; bJ') = e^2 \sum_{t=2,4,6} \Omega_t \left| \langle f^N [\alpha SL] J \| U^{(t)} \| f^N [\alpha' S' L'] J' \rangle \right|^2 \dots \dots \dots (6)$$

The intensity parameters  $\Omega_t$  are phenomenological values which include the effects of the glass matrix on the rare earth ions, e.g., covalency of the rare earth ion sites and local structure in the vicinity of rare earth ions.<sup>(9)</sup>

The oscillator strength for a transition of average frequency  $\nu$  from a  $J$  manifold to a  $J'$  manifold is calculated using the following formula:

$$P_{cal}(aJ; bJ') = \frac{8\pi^2 m \nu}{3h(2J+1)e^2 n^2} \{ \chi_{ed} S_{ed}(aJ; bJ') + \chi_{md} S_{md}(aJ; bJ') \}, \dots \dots \dots (7)$$

where the  $\chi$  terms correct for the effective field at a well-localized center in a medium of isotropic refractive index  $n$ . They are given by  $\chi_{ed} = n(n^2+2)/9$  for electric dipole transitions and  $\chi_{md} = n^3$  for magnetic dipole transitions.

It is difficult to calculate  $\Omega_t$  parameters theoretically since they include contributions from the crystalline electric field, the inter-configurational radial integrals and the average energy separation of the opposite parity configurations. The common way of obtaining the  $\Omega_t$  parameters is to determine the oscillator strength of the transitions by measuring the integrated absorption coefficients. The experimental oscillator strength is derived from measurements of the absorption spectrum using the following equation:

$$P_{mes} = \frac{mc}{\pi e^2 N_{RE}} \int \mu(\nu) d\nu, \dots \dots \dots (8)$$

where  $\mu(\nu)$  is the absorption coefficient at frequency  $\nu$ , and  $N_{RE}$  is the number density of the rare earth ions. Finally, a least-squares-fitting method between Eqs. (4) and (8) is used to find the  $\Omega_t$  parameters that give

the best-fitted oscillator strength. The values of the reduced matrix elements  $\langle \| U^{(t)} \| \rangle$  calculated in an intermediate coupling approximation by Carnall were utilized since these are almost host invariant.<sup>(10,11)</sup> The measure of the quality of the fits is reflected in the root-mean-square deviation  $\delta_{rms}$  between the measured and calculated oscillator strengths:

$$\delta_{rms} = \left\{ \frac{\sum_{i=1}^i (P_{mes} - P_{cal})^2}{i - j} \right\}^{1/2} \dots \dots \dots (9)$$

where  $\sum (P_{mes} - P_{cal})^2$  is the sum of squares of the deviations,  $i$  is the number of transitions, and  $j$  is the number of parameters to calculate (normally three). The spontaneous emission rate between the  $J$  manifolds is given by

$$A(aJ; bJ') = \frac{64\pi^4 \nu^3}{3(2J+1)hc^3} \{ \chi_{ed} S_{ed}(aJ; bJ') + \chi_{md} S_{md}(aJ; bJ') \}, \dots \dots \dots (10)$$

This is related to the radiative lifetime  $\tau_{rad}$  of the excited  $J'$  manifolds by

$$\tau_{rad} = \frac{1}{\sum_{J'} A(aJ; bJ')}, \dots \dots \dots (11)$$

The radiative quantum efficiency  $\eta$  of the level  $J$  is defined as the ratio of the measured lifetime  $\tau_{mes}$  and the radiative lifetime,  $\eta = \tau_{mes}/\tau_{rad}$ . The branching ratio, which is the relative transition strength of the  $J$ - $J'$  transition in all transitions from level  $J$  to a lower lying level  $J'$ , is calculated from

$$\beta_{J'} = \frac{A(aJ; bJ')}{\sum A(aJ; bJ')}, \dots \dots \dots (12)$$

The stimulated emission cross section is given by

$$\sigma_{se} = \frac{\lambda_{pk}^4}{8\pi c n^2 \Delta\lambda_{eff}} A(aJ; bJ'), \dots \dots \dots (13)$$

where  $\lambda_{pk}$  is the wavelength of the emission peak, and  $\Delta\lambda_{eff}$  is the effective line width.  $\Delta\lambda_{eff}$  is defined through the relation

$$I_{pk} \Delta\lambda_{eff} = \int I(\lambda) d\lambda, \dots \dots \dots (14)$$

where  $I_{pk}$  and  $I(\lambda)$  are the emission peak intensity and the emission spectrum, respectively.

The J-O analysis will be utilized to obtain spectroscopic properties of  $Tb^{3+}$ , such as the stimulated emission cross section, the radiative lifetime, and the branching ratio for  $4f-4f$  transitions. ESA can also be estimated by J-O analysis in principle. However, it is difficult to obtain the probability of the excited state absorption from the  $^5D_4$  level of  $Tb^{3+}$  by J-O analysis, since the reduced matrix elements from  $^5D_4$  to the upper levels are unknown. Thus, the ESA effects will be treated by a rigorous analytical model based on the coupled rate equation and on the energy distribution of the pump and signal inside a  $Tb^{3+}$ -doped fiber, as discussed in Section 3.

## 2. 2 Results and discussion

### 2. 2. 1 Absorption spectra

Figure 1 shows an absorption spectrum of the ZBLAN glass doped with 2 wt%  $Tb^{3+}$  at 300 K. Some representative absorption transitions are assigned in Fig. 1. Although it has been reported that an absorption band due to defects involving  $Tb^{4+}$  appears at around 420 nm, such an absorption band was not observed in our samples<sup>(12)</sup>. Thus the Tb ion doping in the ZBLAN

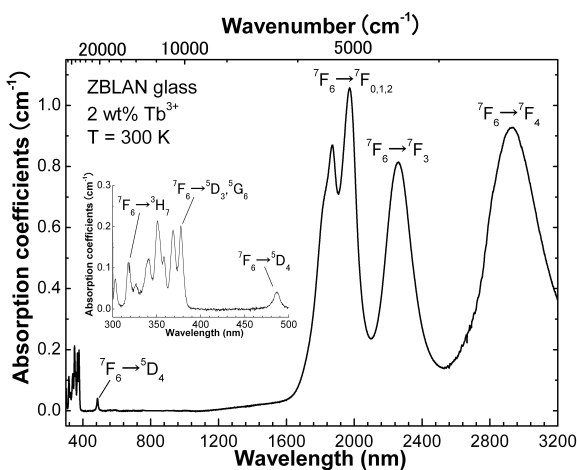


Fig. 1 Absorption spectrum of ZBLAN glass doped with 2 wt% of  $Tb^{3+}$  at 300 K. The inset shows an expansion of the spectrum in the UV-visible wavelength range.

glass was considered to be in a trivalent state. The absorption peaks located at wavelengths of 318, 486, 2263, and 2946 nm were assigned to transitions from the  $^7F_6$  level to the  $^3H_7$ ,  $^5D_4$ ,  $^7F_3$ , and  $^7F_4$  levels, respectively. The three absorption transitions from the ground state, i.e.,  $^7F_6$  to  $^7F_2$ ,  $^7F_1$ , and  $^7F_0$ , overlap in the absorption band located at around 1920 nm. J-O analysis was carried out using the integrated absorption coefficients of these bands.

### 2. 2. 2 Excitation and emission spectra

Figure 2 shows the excitation spectrum of the  $Tb^{3+}:^5D_4 \rightarrow ^7F_5$  emission observed in ZBLAN glass doped with 2 wt%  $Tb^{3+}$  at 300 K monitored at 544 nm. For comparison, the absorption coefficient spectrum is also shown as a dashed line. The excitation spectrum was very similar to the absorption spectrum. It is understood that the  $^5D_4$  level of  $Tb^{3+}$  could be excited via the ( $^5D_3, ^5G_6$ ) levels.

Figure 3 shows the emission spectrum of the ZBLAN glass doped with 2 wt%  $Tb^{3+}$  measured in the visible wavelength range at 300 K. The effective emission band width (FWHM),  $\Delta\lambda_{eff}$ , into the ZBLAN glass is 8.8 nm.

### 2. 2. 3 Judd-Ofelt analysis of $Tb^{3+}$ -doped ZBLAN glass

The J-O analysis was carried out for the ZBLAN doped with 2 wt%  $Tb^{3+}$  as summarized in Table 1. The absorption band at 1920 nm was deconvoluted using Gaussian functions into three absorption bands, due to

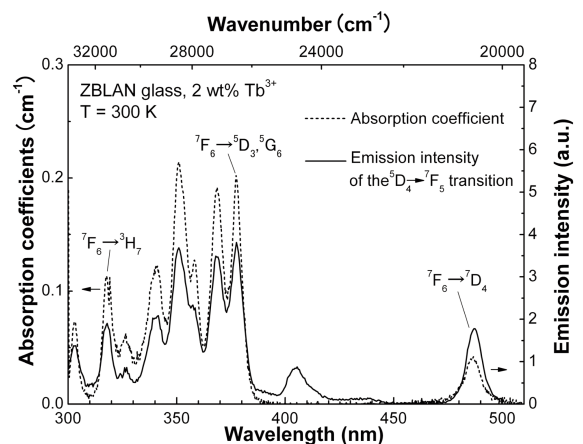
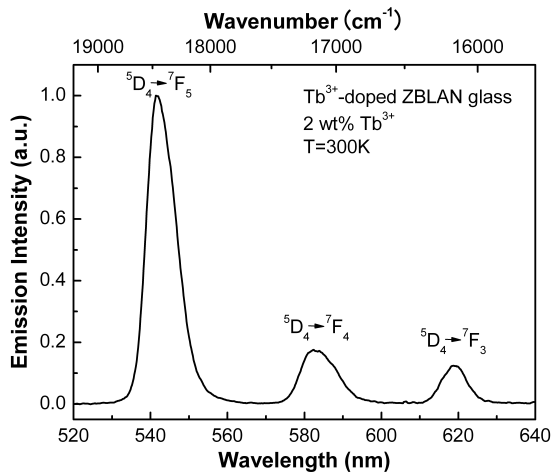


Fig. 2 Excitation spectrum of  $Tb^{3+}$ -doped ZBLAN glass with a  $Tb^{3+}$  concentration of 2 wt% at 300 K.

transitions from the ground state  ${}^7F_6$  to the excited states  ${}^7F_2$ ,  ${}^7F_1$ , and  ${}^7F_0$ , respectively. Using Eq. (8), the seven oscillator strengths for the absorptions from the ground state  ${}^7F_6$  to the excited states  ${}^7F_4$ ,  ${}^7F_3$ ,  ${}^7F_2$ ,  ${}^7F_1$ ,  ${}^7F_0$ ,  ${}^5D_4$ , and  ${}^5H_7$  were obtained experimentally and utilized for the J-O analysis. The intensity parameters  $\Omega_i$  for the ZBLAN doped with 2 wt%  $Tb^{3+}$  were  $\Omega_2 = 2.93 \pm 0.33 \times 10^{-20} \text{ cm}^2$ ,  $\Omega_4 = 5.23 \pm 0.25 \times 10^{-20} \text{ cm}^2$ , and  $\Omega_6 = 2.87 \pm 0.24 \times 10^{-20} \text{ cm}^2$ . In Table 1, the experimental oscillator strengths are compared with



**Fig. 3** Emission spectrum of  $Tb^{3+}$ -doped ZBLAN glass with a  $Tb^{3+}$  concentration of 2 wt% at 300 K.

**Table 1** Experimental and calculated oscillator strengths and the intensity parameters for the ZBLAN doped with 2 wt%  $Tb^{3+}$ .

Absorption	Average frequency ( $\text{cm}^{-1}$ )	Wavelength (nm)	$P_{mes}$ ( $10^{-6}$ )	$P_{cal}$ ( $10^{-6}$ )	
				ed	md
${}^7F_6 \rightarrow {}^7F_4$	3394	2946	1.448	1.405	
${}^7F_6 \rightarrow {}^7F_3$	4420	2263	1.096	1.190	
${}^7F_6 \rightarrow {}^7F_2$	5069	1973	0.969	0.903	
${}^7F_6 \rightarrow {}^7F_1$	5367	1863	0.529	0.645	
${}^7F_6 \rightarrow {}^7F_0$	5563	1798	0.531	0.256	
${}^7F_6 \rightarrow {}^5D_4$	20563	486	0.076	0.024	
${}^7F_6 \rightarrow {}^5H_6$	31456	318	0.158	0.226	0.002
Intensity parameters ( $10^{-20} \text{ cm}^2$ ) rms deviation					
$\Omega_2 = 2.93 \pm 0.18$		$\delta_{rms} = 1.7 \times 10^{-7}$			
$\Omega_4 = 5.23 \pm 0.05$					
$\Omega_6 = 2.87 \pm 0.01$					

the calculated values. The value of  $\delta_{rms}$  was  $1.7 \times 10^{-7}$ , which is comparable to the rms deviations reported for other rare earth-doped materials.

The intensity parameters are compared to those obtained for other glass hosts in **Table 2**. According to previous studies on the compositional dependence of the intensity parameters, the  $\Omega_2$  parameter is affected by the covalency of the Re-O bond, while  $\Omega_6$  is related to the packing density of the rare earth ion.<sup>(13,14)</sup> The obtained  $\Omega_2$  parameter supports the ionic character of fluoride glasses, because the  $\Omega_2$  parameter was the smallest for ZBLAN glasses among all the glasses.

With the  $\Omega_i$  parameters in hand, the spontaneous transition probability  $A_{ed}$ , the branching ratio  $\beta_{JJ}$ , and the radiative lifetime  $\tau_{rad}$  can be calculated. The results of these calculations for ZBLAN glass are summarized in **Table 3**. The radiative lifetime  $\tau_{rad}$  of the  ${}^5D_4$  level was obtained as  $3.92 \pm 0.13 \text{ ms}$  for the ZBLAN glass doped with 2 wt%  $Tb^{3+}$ . The branching ratio of the  ${}^5D_4 \rightarrow {}^7F_5$  transition was found to be 54%, and this transition was the dominant transition from the  ${}^5D_4$  level. The measured lifetime  $\tau_{mes}$  of the  ${}^5D_4$  level was  $3.95 \pm 0.05 \text{ ms}$  and remained almost constant for  $Tb^{3+}$  concentrations below 5 wt% (data not shown). It was found that the quantum efficiency of the  ${}^5D_4 \rightarrow {}^7F_J$  transitions of the  $Tb^{3+}$ -doped ZBLAN glass was about 100% by comparison with the radiative lifetime  $\tau_{rad}$ .

**Figure 4** shows the emission cross sections of the  ${}^5D_4 \rightarrow {}^7F_J$  ( $J = 6, 5, 4, 3$ ) transitions and the absorption cross section of the  ${}^7F_6 \rightarrow {}^5D_4$  transition for the ZBLAN glass doped with 2 wt%  $Tb^{3+}$ . The emission cross sections were calculated using Eqs. (13) and (14). The peak values of the cross sections for several transitions are summarized in **Table 4**. The highest value of the peak emission cross section,  $\sigma_{em}$ , is  $8.1 \times 10^{-22} \text{ cm}^2$  for the  ${}^5D_4 \rightarrow {}^7F_5$  transition in  $Tb^{3+}$ -doped ZBLAN glass. The absorption cross section of the  ${}^7F_6$

**Table 2** The intensity parameters  $\Omega_i$  for different host glasses.<sup>(19)</sup>

$Tb^{3+}$ -doped glass	$\Omega_2$ ( $10^{-20} \text{ cm}^2$ )	$\Omega_4$ ( $10^{-20} \text{ cm}^2$ )	$\Omega_6$ ( $10^{-20} \text{ cm}^2$ )
Fluoride <sup>a</sup>	2.93	5.23	2.87
Borosilicate (5 wt% $Tb^{3+}$ )	6.26	2.39	2.49
Borophosphate	6.55	2.45	3.07
Borate	5.56	1.33	3.22
Phosphate	6.44	1.05	2.21

<sup>a</sup>This work

→ <sup>5</sup>D<sub>4</sub> transition for the 2 wt% Tb<sup>3+</sup>-doped ZBLAN glass was obtained as 1.0 × 10<sup>-22</sup> cm<sup>2</sup>.

The <sup>5</sup>D<sub>4</sub> → <sup>7</sup>F<sub>5</sub> transition of Tb<sup>3+</sup> acts as a four-level laser system, since the <sup>7</sup>F<sub>5</sub> level is about 2200 cm<sup>-1</sup> above the ground level. The gain efficiency *m* (dB/mW) for a four-level laser system is estimated from the following equation:

$$m = \frac{4.34 \sigma_{em} \tau_{mes}}{h\nu_p A_{eff}} \dots \dots \dots (15)$$

where *hν<sub>p</sub>* is the pump photon energy and *A<sub>eff</sub>* is the effective core area.<sup>(15)</sup> The gain efficiency *m* is proportional to the value of *σ<sub>em</sub>τ<sub>mes</sub>*, which is the product of the emission cross section and measured

lifetime. For comparison, we list the *σ<sub>em</sub>τ<sub>mes</sub>* product for several rare earth-doped glasses for which lasing has been observed in **Table 5**.<sup>(19)</sup> The *σ<sub>em</sub>τ<sub>mes</sub>* product of the <sup>5</sup>D<sub>4</sub> → <sup>7</sup>F<sub>5</sub> transition of Tb<sup>3+</sup>-doped ZBLAN glass was 2.8 × 10<sup>-24</sup> cm<sup>2</sup>sec, which is larger than for Tb<sup>3+</sup>-doped borosilicate glass. This value was found to be higher than that of both Tm<sup>3+</sup>-doped fluoride glasses<sup>(16)</sup> and a Pr<sup>3+</sup>-doped fluoride glass,<sup>(17)</sup> whereas it was lower than those of Er<sup>3+</sup>-doped fluoride glasses.<sup>(18)</sup> This high value indicates that this transition has potential as a green laser transition.

### 2.3 Summary

We have investigated the spectroscopic properties of Tb<sup>3+</sup> doped in fluoride glass with a composition of

**Table 3** Predicted spontaneous-radiative transition rates and lifetimes of Tb<sup>3+</sup>-doped ZBLAN glass.

Transition	Average frequency (cm <sup>-1</sup> )	Wavelength (nm)	<i>S<sub>ed</sub></i> (s <sup>-1</sup> )	<i>S<sub>md</sub></i> (s <sup>-1</sup> )	Lifetime		Branching ratio β (%)
					<i>τ<sub>red</sub></i> (ms)	<i>τ<sub>mes</sub></i> (ms)	
<sup>5</sup> D <sub>4</sub> → <sup>7</sup> F <sub>6</sub>	20564	486	24.9		3.92 ± 0.13	3.95 ± 0.05	9.7
→ <sup>7</sup> F <sub>5</sub>	18515	540	88.6	49.2			54.0
→ <sup>7</sup> F <sub>4</sub>	17170	582	20.2	4.7			9.8
→ <sup>7</sup> F <sub>3</sub>	16145	619	11.9	31.0			16.8
→ <sup>7</sup> F <sub>2</sub>	15495	645	5.5				2.1
→ <sup>7</sup> F <sub>1</sub>	15197	658	11.7				4.6
→ <sup>7</sup> F <sub>0</sub>	15001	667	7.6				3.0
<sup>5</sup> D <sub>3</sub> → <sup>7</sup> F <sub>6</sub>	26155	372	361.4		1.77		64.0
→ <sup>7</sup> F <sub>5</sub>	24106	403	7.5				1.3
→ <sup>7</sup> F <sub>4</sub>	22761	426	131.6				23.3
→ <sup>7</sup> F <sub>3</sub>	21736	1585	64.2				11.4
→ <sup>7</sup> F <sub>2</sub>	21086	382	33.5				2.9
→ <sup>7</sup> F <sub>1</sub>	20788	415	96.2				8.3
→ <sup>5</sup> D <sub>4</sub>	5591	439	79.2	61.3			12.1
<sup>5</sup> G <sub>6</sub> → <sup>7</sup> F <sub>6</sub>	26472	460	25.1	731.5	2.12		64.9
→ <sup>7</sup> F <sub>5</sub>	24423	474	53.7	16.7			6.0
→ <sup>7</sup> F <sub>4</sub>	23078	481	30.2				2.6
→ <sup>7</sup> F <sub>3</sub>	22053	1789	18.4	19.4			3.2
→ <sup>7</sup> F <sub>2</sub>	21403	378	204.0	80.4			60.4
→ <sup>7</sup> F <sub>1</sub>	21105	409	135.9	13.4			31.7
→ <sup>7</sup> F <sub>0</sub>	20909	433	31.1				6.6
→ <sup>5</sup> D <sub>4</sub>	5908	453	1.7		0.4		
<sup>5</sup> L <sub>10</sub> → <sup>7</sup> F <sub>6</sub>	26875	467	2.6				0.5
→ <sup>7</sup> F <sub>5</sub>	24826	474	0.0				0.0
→ <sup>7</sup> F <sub>4</sub>	23481	478	1.0				0.2
→ <sup>5</sup> D <sub>4</sub>	6311	1693	0.6				0.1

51ZrF<sub>4</sub>-20BaF<sub>2</sub>-4.5LaF<sub>2</sub>-4.5AlF<sub>3</sub>-20NaF (ZBLAN), which can be used as optical fiber materials. The  $\sigma_{em}\tau_{mes}$  products of the  $^5D_4 \rightarrow ^7F_5$  transitions of Tb<sup>3+</sup>-doped ZBLAN glasses were found to be larger than those of laser transitions in both Tm<sup>3+</sup>- and Pr<sup>3+</sup>-doped fluoride glasses. Thus Tb<sup>3+</sup>-doped ZBLAN glasses are considered as potential candidates for gain media for fiber lasers and amplifiers in the green (0.54  $\mu$ m) band.

### 3. Optical amplification and laser oscillation characteristics of Tb<sup>3+</sup>-doped fiber

In this section, we experimentally evaluated the optical amplification performance of a TBDF in order to understand the amplification mechanism including signal ESA, pump ESA, and cooperative upconversion. To avoid photodarkening and ESAs

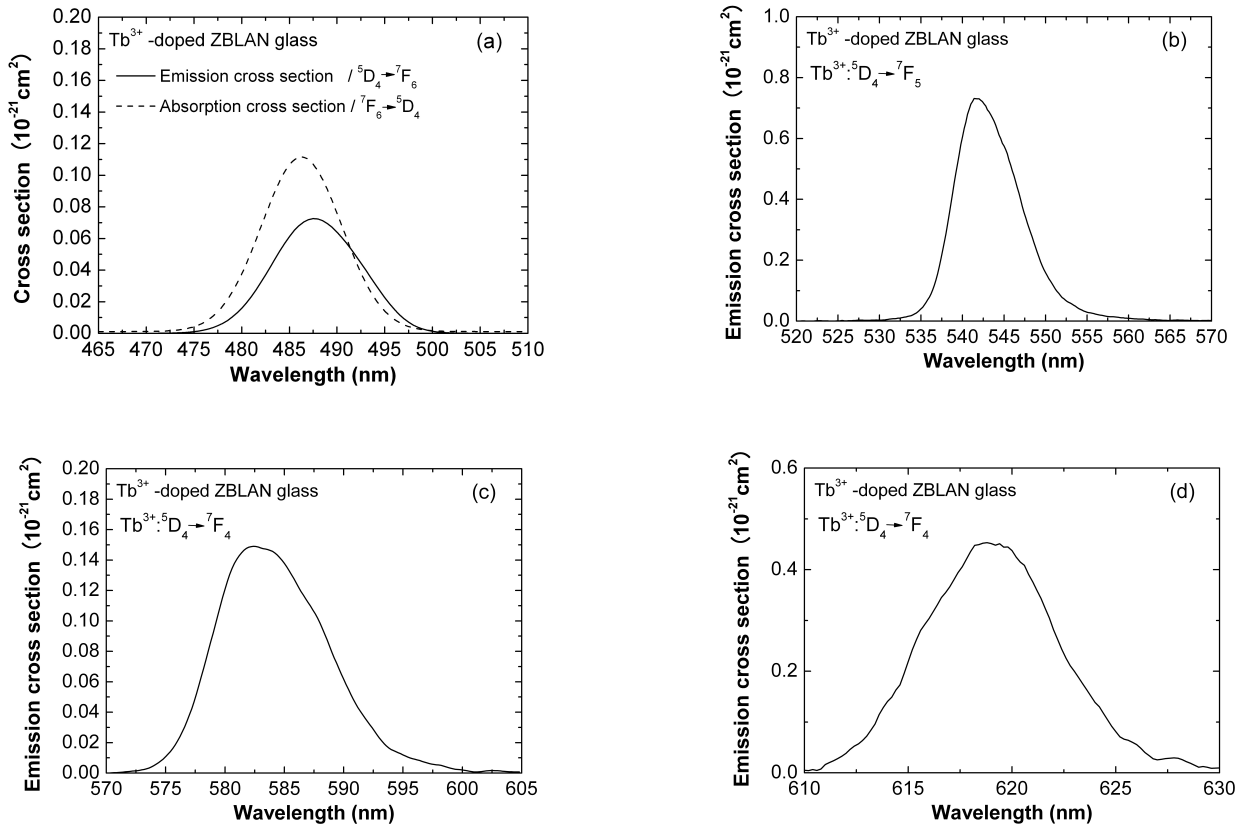


**Fig. 4** Emission cross-section spectra of the (a)  $^5D_4 \rightarrow ^7F_6$  transition, (b)  $^5D_4 \rightarrow ^7F_5$  transition, (c)  $^5D_4 \rightarrow ^7F_4$  transition and (d)  $^5D_4 \rightarrow ^7F_3$  transition of Tb<sup>3+</sup> in ZBLAN glass. The absorption cross-section spectrum of the  $^7F_6 \rightarrow ^5D_4$  transition is also shown in Fig. 4 (a).

**Table 4** The peak values of the absorption and simulated emission cross sections,  $\sigma_a$  and  $\sigma_{em}$ , the peak wavelength,  $\lambda_{pk}$ , and the effective line width,  $\Delta\lambda_{eff}$ , for visible transitions in Tb<sup>3+</sup>-doped ZBLAN glass.

Transition	Absorption			Emission		
	$\lambda_{pk}$ (nm)	$\Delta\lambda_{eff}$ (nm)	$\sigma_a$ (10 <sup>-21</sup> cm <sup>2</sup> )	$\lambda_{pk}$ (nm)	$\Delta\lambda_{eff}$ (nm)	$\sigma_{em}$ (10 <sup>-21</sup> cm <sup>2</sup> )
$^5D_4 \rightarrow ^7F_6$	486	10.1	0.1	488	11.0	0.07
$\rightarrow ^7F_5$				541	9	0.72
$\rightarrow ^7F_4$				582	10.9	0.07
$\rightarrow ^7F_3$				619	9.0	0.45

from the  $^5D_4$  level to the  $5d$  levels, a fluoride fiber was used as a host material for the signal gain measurements, because the  $5d$  levels of  $Tb^{3+}$  would be at higher positions in fluoride materials than in oxide materials. The amplification performance of a  $Tb^{3+}$ -doped fiber operating in the  $0.54 \mu m$  band was demonstrated experimentally, and the gain characteristics of the  $^5D_4 \rightarrow ^7F_5$  transition of the  $Tb^{3+}$ -doped fiber were analyzed using a numerical model. In addition, we demonstrated continuous-wave (CW) laser operation of a TBDF laser at 542.8 nm.

### 3.1 Experimental

#### 3.1.1 Signal amplification experiment

The setup used for the signal amplification experiment is shown in Fig. 5. A TBDF doped with 1 wt% of  $Tb^{3+}$  was used in the signal amplification experiment. The core diameter was  $2.3 \mu m$ , the relative refractive-index difference between the core and the cladding was 0.54%, the cut-off wavelength was

$0.47 \mu m$ , and the fiber length was 5 m. An  $Ar^+$  laser with a wavelength of 488 nm and a green He-Ne laser with a wavelength of 543.5 nm were used as the pump and the signal light source, respectively. The pump and signal lights were coupled to the TBDF by a wavelength-division multiplexing (WDM) coupler. The output signals were detected with an optical spectral analyzer (OSA). The internal gain was obtained from the ratio of the output signal power observed on the OSA when the pump light was coupled to the fiber ( $P_{s,p}$ ) compared to the output signal power without the pump light ( $P_{s,0}$ ), i.e., internal gain =  $10 \log(P_{s,p}/P_{s,0})$ . To obtain the amplified signal power  $P_{p,s}$ , the amplified spontaneous emission (ASE) power was eliminated from the observed spectra.

#### 3.1.2 Fiber laser experiment

The setup for the laser oscillation experiment is shown in Fig. 6. The experiment was carried out using the same TBDF used in the amplification experiments. A Fabry-Perot laser cavity consisted of a TBDF

**Table 5** Comparison of the  $\sigma_{em}\tau_{mes}$  products for rare earth-doped glasses.<sup>(19)</sup>

Rare earth-doped glass	Emission Wavelength (nm)	Radiative lifetime $\tau_{mes}$ (ms)	Emission cross section $\sigma_{em}$ ( $10^{-21} \text{ cm}^2$ )	$\sigma_{em} \tau_{mes}$ ( $10^{-24} \text{ cm}^2 \text{ s}$ )
Er-doped silica glass	1532	11	5	55
Nd-doped fluoride glass	1300	0.45	8	3.6
Tb-doped ZBLAN glass <sup>a</sup>	541	3.95	0.72	2.8
Tm-doped fluoride glass	480	1.6	1.12	1.8
Pr-doped fluoride glass	1300	0.11	3.5	0.4

<sup>a</sup> This work

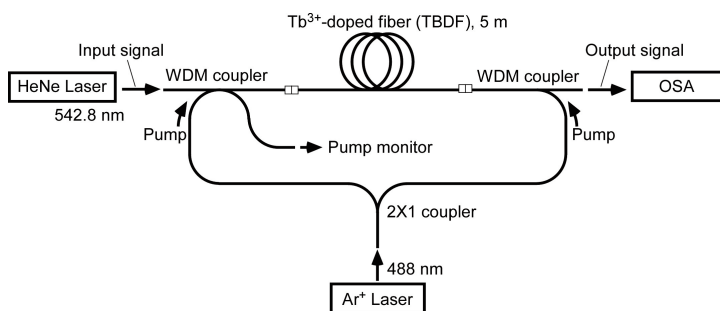


**Fig. 5** Experimental setup for signal amplification of  $Tb^{3+}$ -doped fiber.

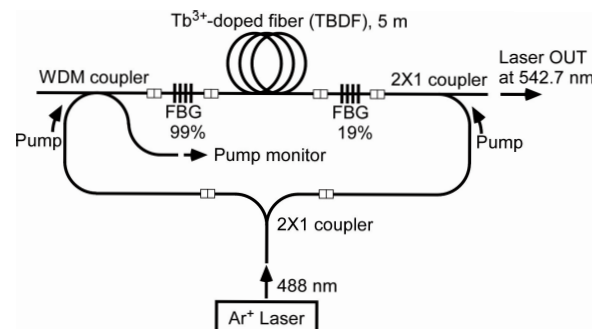


**Fig. 6** Experimental setup for lasing of  $Tb^{3+}$ -doped fiber.

connected by fiber Bragg gratings (FBGs) with reflectivities of 99% (as a high reflector) and 19% (as an output coupler) at 542.8 nm.

### 3.2 Results and discussion

#### 3.2.1 Amplification characteristics of Tb<sup>3+</sup>-doped fluoride fiber at 543 nm

Figure 7 shows the ASE spectra of the <sup>5</sup>D<sub>4</sub> → <sup>7</sup>F<sub>5</sub> transition in the TBDF. When the launched pump power was increased, the peak wavelength remained constant at 541.8 nm, however, narrowing of the emission spectral bandwidth was observed. Figure 8 shows the relationship between the small-signal gain and the pump power for the TBDF. The input signal power was -30 dBm. The signal gains shown in Fig. 8 were obtained from the internal gain by subtracting a fiber propagation loss of 0.043 dB/m at 544 nm. In the case of forward pumping, a signal gain of 5.2 dB was obtained at a pumping power of 115 mW.

The solid and dashed lines in Fig. 8 show the calculated signal gain dependence on pump power. In this calculation, we use the spectroscopic parameters of the Tb<sup>3+</sup>-doped ZBLAN glass obtained in the previous section and include these in an amplification model of the TBDF taking into account the effects of ESA and cooperative upconversion.<sup>(20)</sup> The transition probabilities of pump and signal ESA transitions cannot be obtained by J-O analysis because the reduced matrix elements for these transitions are unknown. In addition, since absorption bands due to the 5*d* levels of Tb<sup>3+</sup> would be below 40,000 cm<sup>-1</sup>, the

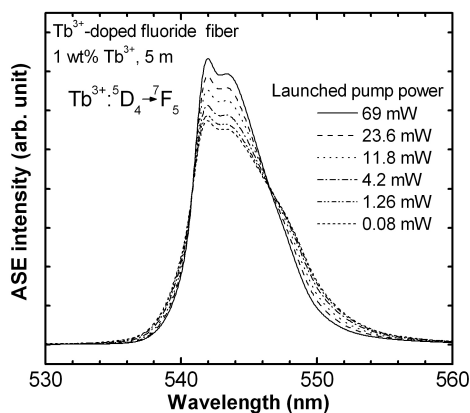


Fig. 7 Variation in ASE spectra for the <sup>5</sup>D<sub>4</sub> → <sup>7</sup>F<sub>5</sub> transition at various pump powers. The ASE intensities were normalized to be equal for comparison.<sup>(20)</sup>

signal ESA, pump ESA and cooperative upconversion would be caused by transitions from the <sup>5</sup>D<sub>4</sub> level to the 5*d* levels.

If the contributions from the ESAs and cooperative upconversion are ignored, the gain will increase monotonically, as shown by the dashed line. However, the experimental gain characteristics indicate a tendency to saturate with increasing pump power. The absorption cross sections for the pump ESA, the signal ESA and the upconversion coefficient were chosen such that the calculated gains could fit the measured gains. When the cross section of the pump ESA was  $1.34 \times 10^{-22}$  cm<sup>2</sup>, the calculated gains agreed well with the measured values. Even when considering the signal ESA and the effects of cooperative upconversion, no improvements in the fitted results could be made. Thus, the signal amplification performance for the TBDF is thought to be dominated by the pump ESA. The pump ESA would be caused by the absorption to the 5*d* levels of Tb<sup>3+</sup>, which are below 40,000 cm<sup>-1</sup>.

Figure 8 also shows the relationship between the signal gain and pump power for a bi-directional pump scheme. A signal gain of 8.3 dB was obtained at a pumping power of 130 mW. It was found that the signal gain could thus be enhanced by adopting bi-

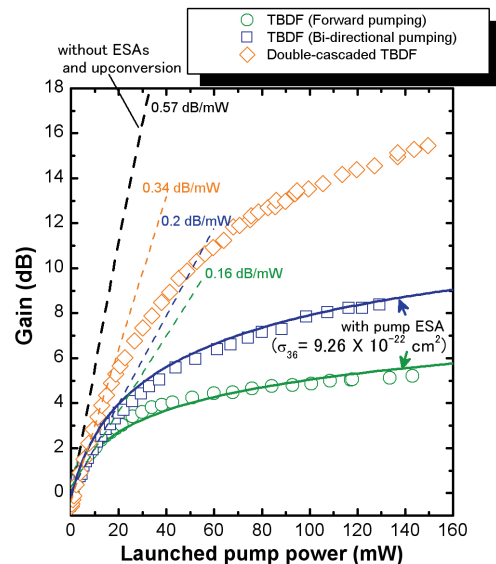
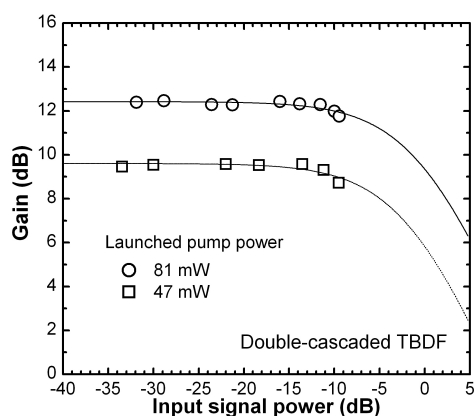


Fig. 8 Dependence of gain on pump power for single and double-cascaded TBDFs. The solid green and blue lines are the calculated results for the forward and bi-directional pumped TBDFs, respectively. The dashed lines show the gain coefficient obtained from the initial slope of the pump power dependence.<sup>(20)</sup>

directional pumping as compared to forward pumping. Since the strength of the pump ESA has a quadratic dependence on the pump power, this result points to undesirable pump ESA effects influencing the amplification process in the TBDF. Therefore, we believe that side-pumping schemes with double-cladding fiber structures would be suitable for TBDF lasers and amplifiers because this would realize a more gradual distribution of pump power along the fiber than that obtained for the end pumping scheme.

In addition, we constructed a double-cascaded TBDF (Tb<sup>3+</sup>-doped fiber amplifier) that included two pieces of TBDF. As shown in Fig. 8, a signal gain of 15.5 dB was obtained at a pumping power of 150 mW for the double-cascaded TBDF, which was almost twice that obtained for the bi-directional pumping system with the same total pumping power. **Figure 9** shows the variation in the gain of the TBDF with respect to input signal power at two different pump powers. The gain characteristics were flat for input signal powers between -33 dBm and -17 dBm. The solid lines in Fig. 9 show the gain ( $g$ ) calculated using the relationship  $g = g_0(1 + P_s/P_{sat})^{-1}$ , where  $g_0$  is the small-signal gain and  $P_{sat}$  is the saturation signal power for 3 dB gain compression. The saturated signal powers at pump powers of 47 mW and 81 mW were the same, and were about 0 dBm. This shows that the TBDF behaves as a four-level system.

Atkins et al. have observed photo-darkening effects resulting from increases in absorption in the visible wavelength region due to the photo-ionization of Tb<sup>3+</sup> to Tb<sup>4+</sup> in Tb<sup>3+</sup>-doped germanosilicate and phosphosilicate fibers with 488 nm excitation.<sup>(5)</sup>



**Fig. 9** Dependence of gain on signal power for a double-cascaded TBDF using bi-directional pumping.<sup>(20)</sup>

However, no such effects were observed during our experiment, and the background loss of the TBDF used did not change before and after the experiments. The photo-ionization effect would occur when the 5d levels of Tb<sup>3+</sup> are optically excited.<sup>(5)</sup> This result suggests that the 5d absorption bands of Tb<sup>3+</sup> doped in ZBLAN glass occupy higher energy levels and/or are weaker than those in silicate glasses so that the amplification phenomenon of the <sup>5</sup>D<sub>4</sub> → <sup>7</sup>F<sub>5</sub> transition in TBDF has been observed and this is the reason amplification of the <sup>5</sup>D<sub>4</sub> → <sup>7</sup>F<sub>5</sub> transition could be observed in the TBDF.

### 3.2.2 Laser oscillation characteristics of Tb<sup>3+</sup>-doped fluoride fiber

**Figure 10** shows the lasing characteristics of the TBDF laser in CW operation with 488 nm pumping at room temperature. The laser was operated at 542.8 nm, which coincides with the FBG wavelength. The threshold was found to be 60 mW, and the fiber laser output power reached 0.28 mW at a 128 mW launched pump power. The slope efficiency was 0.41%. This high threshold is due to the connection losses between the FBGs and the TBDF, and an insertion loss from the WDM coupler. Optimization of the reflectivity of the FBG for signal wavelength, fiber length and also cavity loss would much improve the laser performance.

### 3.3 Summary

In summary, we have demonstrated for the first time optical signal amplification using a TBDF. The pump

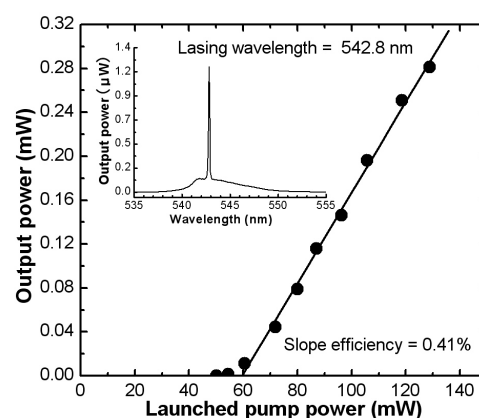


**Fig. 10** Dependence of TBDF laser output on pump power. The inset shows the laser spectrum just above the threshold.<sup>(20)</sup>

ESA was found to dominate the gain characteristics of the  $^5D_4 \rightarrow ^7F_5$  transition in the TBDF with 488 nm pumping. The amplification performance could be improved by adopting bi-directional pumping. In addition, operation of a  $Tb^{3+}$ -doped fiber laser with a Fabry-Perot laser cavity configuration has been demonstrated. This the first time a CW laser operating at 542.8 nm has been successfully demonstrated using a TBDF. These results confirm the potential of TBDFs for use in fiber lasers and fiber amplifiers in the 0.54  $\mu m$  band.

#### 4. Conclusion

The obtained results demonstrate the considerable potential application of  $Tb^{3+}$ -doped fibers in fiber lasers and fiber amplifiers in the 0.54  $\mu m$  band. We have successfully demonstrated continuous-wave laser operation of a  $Tb^{3+}$ -doped fluoride fiber laser at 542.8 nm. Efficient fiber lasers and optical amplifiers using  $Tb^{3+}$ -doped fibers would be feasible, particularly considering the progress in violet-blue laser diode technology. In addition, the problem of pump ESA in the gain led to new insights into the efficient amplifying operation of a  $Tb^{3+}$ -doped fiber amplifier, and a double-cladding structure as well as high doping of  $Tb^{3+}$  ions was found to be effective. The present study is an important step toward the developments of optical amplification devices and fiber lasers for the green band.

#### Reference

- (1) *Rare Earth-doped Fiber Lasers and Amplifiers*, Ed. by Dignonnet, M. J. F. (1993), Marcel Dekker, Inc.
- (2) Kato, S., et al., *R&D Review of Toyota CRDL*, Vol.40, No.2 (2005), pp.7-10.
- (3) Auzel, F., "Upconversion and Anti-stokes Processes with f and d Ions in Solids", *Chem. Rev.*, Vol.104, No.1 (2004), pp.139-174.
- (4) Bjorklund, S., et al., "Laser Action from Terbium Trifluoroacetylacetonate in P-dioxane and Acetonitrile at Room Temperature", *Appl. Phys. Lett.*, Vol.10, No.5 (1967), pp.160-162.
- (5) Atkins, G. R. and Carter, A. L. G., "Photodarkening in  $Tb^{3+}$ -doped Phosphosilicate and Germanosilicate Optical Fibers", *Opt. Lett.*, Vol.19, No.12 (1994), pp.874-876.
- (6) Dorenbos, P., "The 5d Level Positions of the Trivalent Lanthanides in Inorganic Compounds", *J. Lumin.*, Vol.91, No.3/4 (2000), pp.151-176.
- (7) Judd, B. R., "Optical Absorption Intensities of Rare-earth Ions", *Phys. Rev.*, Vol.127, No.3 (1962), pp.750-761.
- (8) Ofelt, G. S., "Intensities of Crystal Spectra of Rare-earth Ions", *J. Chem. Phys.*, Vol.37, No.3 (1962), pp.511-520.
- (9) Peacock, R. D., "The Intensities of Lanthanide f $\leftrightarrow$ f Transitions", *Structure and Bonding* 22 (1975), Springer-Verlag.
- (10) Caird, J. A., et al., "The Terbium Chloride-aluminum Chloride Vapor System. II.", *J. Chem. Phys.*, Vol.74, No.2 (1981), pp.805-812.
- (11) Carnall, W. T., et al., *Argonne National Laboratory Report* (1977), Argonne.
- (12) Reiseberg, L. A. and Moss, H. W., "Multiphonon Orbit-lattice Relaxation of Excited States of Rare-earth Ions in Crystals", *Phys. Rev.*, Vol. 174, No.2 (1968), pp.429-438.
- (13) Layne, B. C., et al., "Multiphonon Relaxation of Rare-earth Ions in Oxide Glasses", *Phys. Rev. B*, Vol.16, No.1 (1977), pp.10-20.
- (14) Layne B. C. and Weber, M. J., "Multiphonon Relaxation of Rare-earth Ions in Beryllium-fluoride Glass", *Phys. Rev. B.*, Vol.16, No.7 (1977), pp.3259-3261.
- (15) Dignonnet, M. F., "Closed-form Expressions for the Gain in Three- and Four-level Laser Fibers", *IEEE J. Quantum Electron.*, Vol.26, No.10 (1990), pp.1788-1796.
- (16) Duclos, F. and Urquhart, P., "Thulium-doped ZBLAN Blue Upconversion Fiber Laser: Theory", *J. Opt. Soc. Am. B*, Vol.12, No.4 (1995), pp.709-717.
- (17) Miyajima, Y., "Erbium- and Neodymium-doped Fluoride Glass Fiber Lasers and Amplifiers", *Proceeding of SPIE 1581*, Ed. by Dignonnet, M. J. and Snizer, E. (1991), pp.304-313, SPIE.
- (18) Miniscalco, W. J., et al., "The Measurement and Analysis of Cross Sections for Rare-earth-doped Glasses", *Proceeding of SPIE 1581*, Ed. by Dignonnet, M. J. and Snizer, E. (1991), pp.80-90, SPIE.
- (19) Yamashita, T. and Ohishi, Y., "Concentration Effects on the Spectroscopic Properties of  $Tb^{3+}$ -doped Borosilicate Glasses", *J. App. Phys.*, Vol.102, No.12 (2007), 1231107.
- (20) Yamashita, T. and Ohishi, Y., "Amplification and Lasing Characteristics of  $Tb^{3+}$ -doped Fluoride Fiber in the 0.54  $\mu m$  Band", *Jpn. J. App. Phys.*, Vol.46, No.41 (2007), pp.L991-L993.

Figs. 7-10

Reprinted from *Jpn. J. Appl. Phys. Part 2*, Vol.46, No.41 (2007), pp.L991-L993 (DOI: 10.1143/JJAP.46.L991), Yamashita, T. and Ohishi, Y., Amplification and Lasing Characteristics of  $Tb^{3+}$ -doped Fluoride Fiber in the 0.54  $\mu m$  Band, © 2007 JSAP, with permission from the Japan Society of Applied Physics.

**Tatsuya Yamashita**

Research Fields :

- Photonic integrated circuits
- Optical communication systems

Academic Degree : Dr. Eng.

Academic Societies :

- IEICE
- The Japan Society of Applied Physics
- The Optical Society of Japan
- The Optical Society of America

Awards :

- Young Scientist Award for the Presentation of an Excellent Paper on the 11th JSAP, 2001
- Best Paper Award of IEICE, 2008
- Best Paper Award of IEEE CPMT Symposium Japan, 2010

**Yasutake Ohishi\***

Research Field :

- Photonics

Academic Degree : Dr. Eng.

Academic Societies :

- The Optical Society of America
- IEEE Photonics Society
- IEICE
- The Japan Society of Applied Physics
- The Ceramics Society of Japan

Awards :

- Best Paper Award of IEICE, 1994
- Best paper Award of 2nd Optoelectronics & Communications Conference (OECC), 1997
- Sakurai Award of Optoelectronic Industry and Technology Development Association (OITDA), 1997
- Electronics Society Award of IEICE, 1998
- Achievement Award of IEICE, 2001
- Academic Award of The Ceramic Society of Japan, 2007

---

\*Toyota Technological Institute